Journal of Sedimentary Research

Journal of Sedimentary Research, 2007, v. 77, 965–979
Research Article
DOI: 10.2110/jsr.2007.086

PROCESS-LIKE MODELING OF FLANK-MARGIN CAVES: FROM GENESIS TO BURIAL EVOLUTION

RICHARD LABOURDETTE,[1] IOAN LASCU,[2,*] JOHN MYLROIE,[2] AND MONICA ROTH[2,†]
[1]*Structural Geology, Sedimentology and Geology Laboratory, TOTAL S.A., Pau, France*
[2]*Department of Geosciences, Mississippi State University, Mississippi State, Mississippi 39762, U.S.A.*
e-mail: richard.labourdette@total.com

ABSTRACT: **A major challenge in groundwater and petroleum modeling is how to represent the diagenesis effect "*sensu lato*" and its associated features (e.g., karst cavities, porosity and permeability characteristics). Both geometrical descriptions and genesis are necessary for modeling diagenetic features, because they allow the restitution of phenomenon in subsurface settings where they cannot be fully observed.**

This study focuses on flank-margin caves developed on carbonate islands (as in the case of the Bahamian islands). Over the last twenty years numerous measurements and observations have been carried out on Quaternary carbonate islands. These, together with reasonable hypotheses of genesis (fresh-water lens dissolution), make island karst an appropriate subject for developing concepts and modeling methods which can be then applied to other diagenetic features, such as reflux dolomitization and hydrothermal fluid effects.

The speleogenesis of flank-margin caves was modeled following deterministic and stochastic methods to achieve a description of dissolution genesis. A fresh-water lens surface was built based on the topography of Long Island, Bahamas, and was then used to simulate virtual development of flank-margin caves at several formation phases, including uncertainty coefficients applied to both fresh-water-lens location and stability time by using 3D probability cubes. The cave simulations were compared with over sixty Bahamian cave surveys, in order to substantiate our modeling processes and results.

Finally, the model was exposed to a cave collapse situation. The likelihood of preservation and the extent of the area affected were measured to provide an evaluation of the spatial distribution of associated petrophysical characteristics (e.g., porosity and permeability).

The results reveal close resemblance and coherence between modeled and field data (including collapse features). Therefore the optimum method for restituting diagenetic features is by stochastic modeling actively driven by process concepts and most up-to-date methods.

INTRODUCTION

The Bahamian Islands are known for their caves and karst features; which have been studied extensively over the past two decades (Mylroie 1983; Palmer et al. 1986; Mylroie and Carew 1988, 1990; Mylroie et al. 1991; Mylroie et al. 1995; Mylroie et al. 2001; Mylroie et al. 2004). The speleogenesis of Bahamian caves is difficult to determine, especially when focusing on duration and development processes. The most significant speleogenetic mechanism seems to be linked to mixing dissolution in fresh-water lens margin during the last interglacial sea-level highstand (Carew and Mylroie 1995).

In spite of the relatively recent eolian morphology of Bahamian Islands (Beach and Ginsburg 1980), Bahamian flank-margin caves exhibit the same characteristic features as those developed in islands dominated by elevated marine limestone deposits, e.g., Isla de Mona (Frank et al. 1998) or Mariana Islands (Jenson et al. 2006). It is possible that a low-relief exposed platform might produce a slightly different cave morphology. This study aims to model the processes related to formation and evolution of flank-margin caves. Although the origins of modern cave and paleocave systems are well documented (*inter alia*, (White 1988; Palmer 1991; Loucks and Handford 1992), little data is available on the internal structure of paleocave hydrocarbon reservoirs at the interwell scale (Loucks and Mescher 1996). Hydrocarbon-bearing paleocave reservoirs in the lower Ordovician Ellenburger and Siluro-Devonian strata of West Texas are well documented and provide conceptual distributions of these internal cave structures (Loucks and Anderson 1985; Kerans 1988; Candelaria and Reed 1992; Holtz and Kerans 1992; Loucks and Handford 1992; Stoudt 1996). White (1988) and Loucks (1999a) describe collapsed caves formed as turbulent stream conduits in continental settings within dense and recrystallized telogenetic rock (the epigenic caves of Palmer 1991). The caves of the Bahamas are formed as mixing chambers in a hypogenic environment in eogenetic rocks with primary porosity usually with values of around 30%. Therefore the collapse of flank-margin caves and banana-hole caves may operate under conditions different from those discussed in previous literature. Several authors agree that karst systems on carbonate platform margins can be preserved (e.g., Briggs and Seiders 1972; Craig 1988; Mylroie 1993; Wilson 1994) even if their vulnerable position can lead to destruction by bank-margin

* Present address: Department of Geology and Geophysics, University of Minnesota, Minneapolis, Minnesota 55455, U.S.A.

† Present address: HydroEnvironmental Solutions, Inc, Somers, New York 10589, U.S.A.

 1527-1404/07/077-965/$03.00

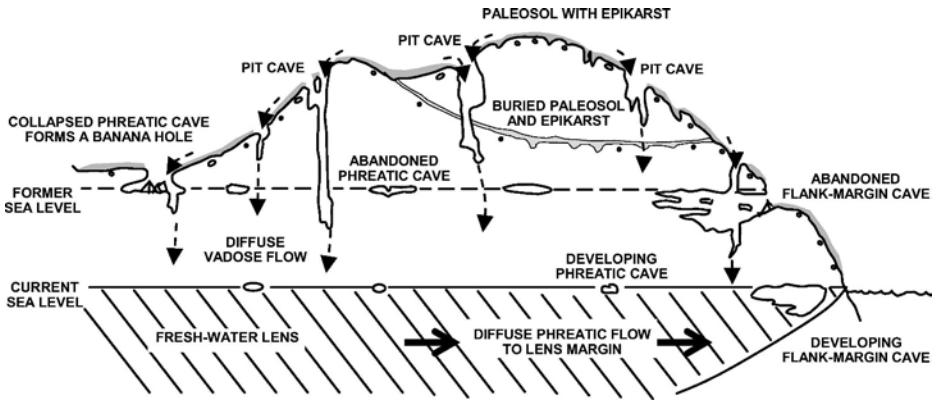

FIG. 1.—Diagrammatic representation of a carbonate island showing the main carbonate-island karst features. Surface water excavates vadose pit caves by downward dissolution, the water eventually continuing by diffuse flow through the remainder of the vadose zone to the fresh-water lens. Diffuse flow in the phreatic zone excavates flank-margin caves by mixing dissolution at the margin of the lens. Isolated phreatic voids also dissolve at the top of the lens: on collapse, they form banana holes. Banana holes and flank-margin caves are controlled by sea-level position, but vadose pit caves at high elevations are independent of sea-level position. In some cases, vadose pit caves intersect flank-margin caves formed during earlier sea-level highstands (from Mylroie and Carew 1995a).

failure or other weathering processes (Mylroie and Carew 1991, 1995b). Loucks (1999b) discussed void survival at depth. Meyerhoff and Hatten (1974) report voids intersected by deep drilling in the Bahama Banks at a depth of 4082 m. Flank-margin caves can be preserved by simple subsidence or by minor eustatic changes. In as much these caves form in the same environment as limestone deposition, they can be quickly buried, whereas telogenetic caves can be buried only by rapid tectonic adjustment.

A second aspect of cave collapse is removal of the debris by continued dissolution. Ford (1995) argues that senescent hypogenic caves (aging surface-isolated caves) could attract speleogenetic fluids and undergo further dissolution, which could include removal of collapse debris. Landmark studies of continental caves (e.g., Ford 1995) provide valuable insights into collapse processes which were incorporated into our simulations, despite not being a perfect analog for Bahamian caves.

This paper demonstrates how object modeling can be driven by sedimentological concepts derived from real observations of cave morphology. Object-based models (boolean simulations) are arrangements of populations of geometric objects in space. In reservoir modeling, boolean simulations are often used to describe clearly identified geological objects, e.g., fracture networks, meandering channel systems, or other sedimentary bodies. Object-based models, unlike pixel-based models, can provide geologically realistic representations of reservoir heterogeneities (Hu 2003) and depend on only a few parameters describing the number of seed points per unit space (density). Object models can be conditioned, by the use not only of probability cubes but also the shape of the modeled objects (fixed or variable), their size, and their orientation. The model can be locally modified in order to reproduce the real phenomenon more accurately (Matheron et al. 1987).

Our modeling workflow reproduces flank-margin cave speleogenesis, spatial distribution and evolution with burial. This workflow is based on the transposition of the different processes of evolution of flank-margin caves, using simple deterministic and stochastic methods by constraining object-based boolean simulations.

CARBONATE ISLAND KARST MODEL AND SPELEOGENESIS

The Carbonate Island Karst Model (CIKM) (Mylroie and Carew 1995b; Mylroie et al. 1995; Mylroie et al. 2001; Mylroie et al. 2004) explains karst development on young carbonate islands, which differs substantially from continental telogenetic karst. Karst formation is intrinsically tied to the presence of a fresh-water lens which is induced by the hydrology of these particular carbonate islands. Due to its density contrast this fresh-water lens floats on saline groundwater. The Dupuit-Ghyben-Herzberg model (Vacher 1988) characterizes the configuration of a fresh-water lens and assumes that its depth at any point below sea level is 40 times its height above sea level. The total thickness of the lens is determined by the quantity of meteoric recharge and permeability of the aquifer; the size and topographic expression of the host landmass act as limiting factors. The lens can be distorted by lithological boundaries, such as terra-rossa paleosols (Mylroie and Carew 1995b).

Flow through the fresh-water lens is diffuse, and discharge into the sea occurs at its distal margin. If the transition between the lens and the saline groundwater is sharp, the contact is called the halocline. If the transition is a broad zone where mixing of fresh water and salt water occurs at a wide interface, this is called the mixing zone. Mixing occurs not only at the bottom of the lens but also at the vadose–phreatic interface, where percolating meteoric water reaches the water table. Field measurements or laboratory experiments demonstrate that when two aqueous solutions, initially saturated in different conditions with respect to calcium carbonate, are mixed, the resulting solution will be undersaturated in $CaCO_3$ (Plummer 1975; Bögli 1980; Dreybrodt 2000). Therefore, the two geochemical mixing environments of the fresh-water lens also have a high dissolutional potential. At the lens margin, where the top and bottom mixing interfaces become superimposed, they create an environment of exceptional dissolution potential.

The Bahamian islands are classified as simple carbonate islands, with carbonate rocks extending well below the depth of the fresh-water lens. The non-carbonate basement does not affect the hydrology or modern geologic development of the islands (Mylroie et al. 2001). Karstic features in the Bahamas include karren, depressions, pit caves, water-table caves (phreatic, banana holes), lake drains, flank-margin caves, and blue holes (Fig. 1; Mylroie and Carew 1995a). Flank-margin caves, based on areal footprint, are the largest karst features found in the Bahamas. They form under the flank of the enclosing land mass, at the margin of the fresh-water lens where dissolution, due to fresh-water–salt-water mixing, is superimposed onto vadose–phreatic mixing. This creates an ideal environment for cave formation. In some cases dissolution is enhanced by oxidation of decaying organic matter trapped at the lens interface (Bottrell et al. 1993).

The long-term tectonic stability of the Bahamas—the only movement is isostatic subsidence of 1–2 m per 100,000 years (McNeill 2005)—means that phreatic caves, found above today's sea level, must have formed at higher sea levels, associated with periods of greater ice melt in polar regions. The fresh-water lens was at elevation of up to six meters above today's sea level for at least 12,000 years during the last interglacial (Oxygen Isotope Substage 5e, ~ 131–119 ka; Chen et al. 1991). This most recent interglacial is believed to have been the major phreatic speleogenetic event, and its results can be observed on dry land today in the Bahamas (Carew and Mylroie 1995).

Flank-margin caves are classified as hypogenic caves (Palmer 1991) and are not directly connected to the surface hydrology. Typically, flank-margin caves are dominated by large globular chambers, broad on the horizontal plane and vertically restricted. They form as closed mixing

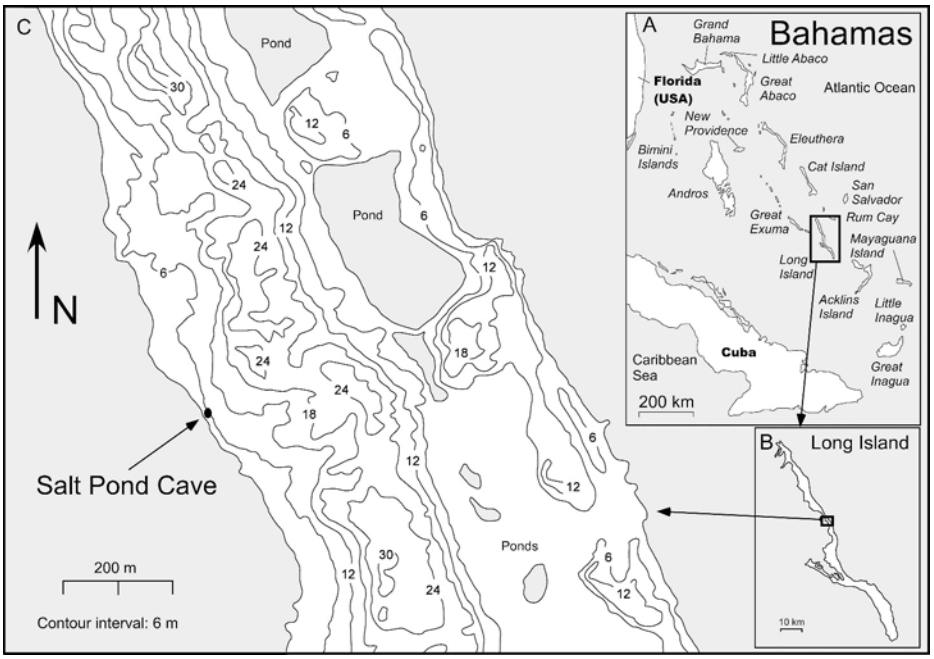

FIG. 2.—**A)** Map of Bahamas Islands, **B)** map of Long Island with **C)** approximate location of Salt Pond Cave (modified from "Operational Navigation Chart" 1974).

chambers in which the reacting solutions enter by diffuse flow; true conduit flow is absent. As they become progressively larger, the mixing front migrates inland, towards the back of the chambers, following preferential pathways which coincide with discrete fresh-water inflow routes (Mylroie and Carew 1990). Flank-margin caves form with no macroscopic connection to the surface environment, i.e., no entrance. Surface erosion creates an entrance by breaching into the cave after formation. Roth (2004) showed that flank-margin caves are statistically distributed into three categories, according to their areal footprint: small (< 100 m^2), medium (100–1000 m^2), and large (> 1000 m^2). The caves are not linear conduits formed by turbulent flow; they have developed in the vertically-restricted lens margin; areal footprint is therefore the most efficient way of assessing cave size. All of the caves originate at the microscopic scale, creating a network of interconnecting pores. As the voids get larger they tend to intersect each other, thereby creating globular, vertically-restricted, small caves (Loucks 1999a). Clustering of small caves results in formation of medium then large caves. As they increase in size, the pattern of development of flank-margin caves becomes more predictable, in the sense that very large caves will have linear areal footprints, "mimicking" their original lens-margin position. The most important condition for development of large caves is a significant stability time in a mixing-zone environment (Roth 2004). Dissolution amounts are partly time-dependent; a continuously moving lens would leave only a small dissolution signal in the rock, unless the rate of movement was slower than the rate of dissolution. In Quaternary systems, fast sea-level variations linked to glacial cycles prohibit the development of macroscopic voids. Flank-margin caves can be found only at the highstand and lowstand glacioeustatic sea-level positions, if the "turn-around" time is long enough (Carew and Mylroie 1995).

Due to the vulnerable position of flank-margin caves at the margin of carbonate platforms, their preservation is constantly being debated (Mylroie and Carew 1995b). The collapse of some shallow caves observed in the Bahamas has generated specific geomorphic features, called "banana holes." The name originates from the use of these sinkholes for agricultural purposes (Jackson 1987). Banana holes are characteristic karst features developed at the top of a past fresh-water lens (Harris et al. 1995). These caves develop over the broad areal extent of the fresh-water lens and are consequently quite common; banana hole densities of over 3,000/km^2 have been reported (Harris et al. 1995). The original voids develop at the top of the fresh-water lens in a setting where the topography is of low relief so the cave roofs are very thin and prone to collapse. However, where the distance between the top of the lens and the land surface is greater, for example on Isla de Mona (Puerto Rico), the expression of banana holes as collapse features decreases dramatically (Frank et al. 1998). Mylroie and Carew (1995b) argue that flank-margin caves are also vulnerable to collapse because they tend to develop near the flank of the land mass enclosing them. Shoreline retreat by normal erosion processes can cause breach of the caves. Flank-margin caves and banana holes form rapidly after sedimentation; thus their preservation is most likely in the case of rapid burial caused by platform subsidence or sea-level rise.

MORPHOLOGY OF FLANK-MARGIN CAVES: A CASE STUDY

To illustrate morphology of flank-margin caves and in order to have a basis for comparison with simulated caves, a 3D reconstruction was carried out using survey data from Salt Pond Cave, Long Island, Bahamas. Long Island is situated at the easternmost edge of the Great Bahama Bank. It is characteristic of the windward islands, with an elongate morphology extending northwest–southeast for more than 100 km. Salt Pond Cave lies just north of Salt Pond Settlement (Fig. 2) and is one of the largest flank-margin caves found on Long Island. The cave has two large chambers separated by a thin wall partition. The main chamber has a volume of 15,540 m^3 from which rock was removed by dissolution at a rate of more than 1 m^3 per year during the last interglacial (Mylroie et al. 1991). A short tunnel, 3 m wide, connects the two chambers (Fig. 3), indicating that the cave developed inland from the lens margin (Mylroie et al. 1995); however, it might also indicate a sudden inland shift of the fresh-water lens (Roth 2004). The morphology of this cave is typical of a flank-margin cave, with globular, vertically restricted, laterally extensive chambers, bedrock pillars, dissolution pockets, and wall sculpture (Fig. 3). Salt Pond Cave was used as a reference for 3D modeling because it is large and has a characteristic morphology.

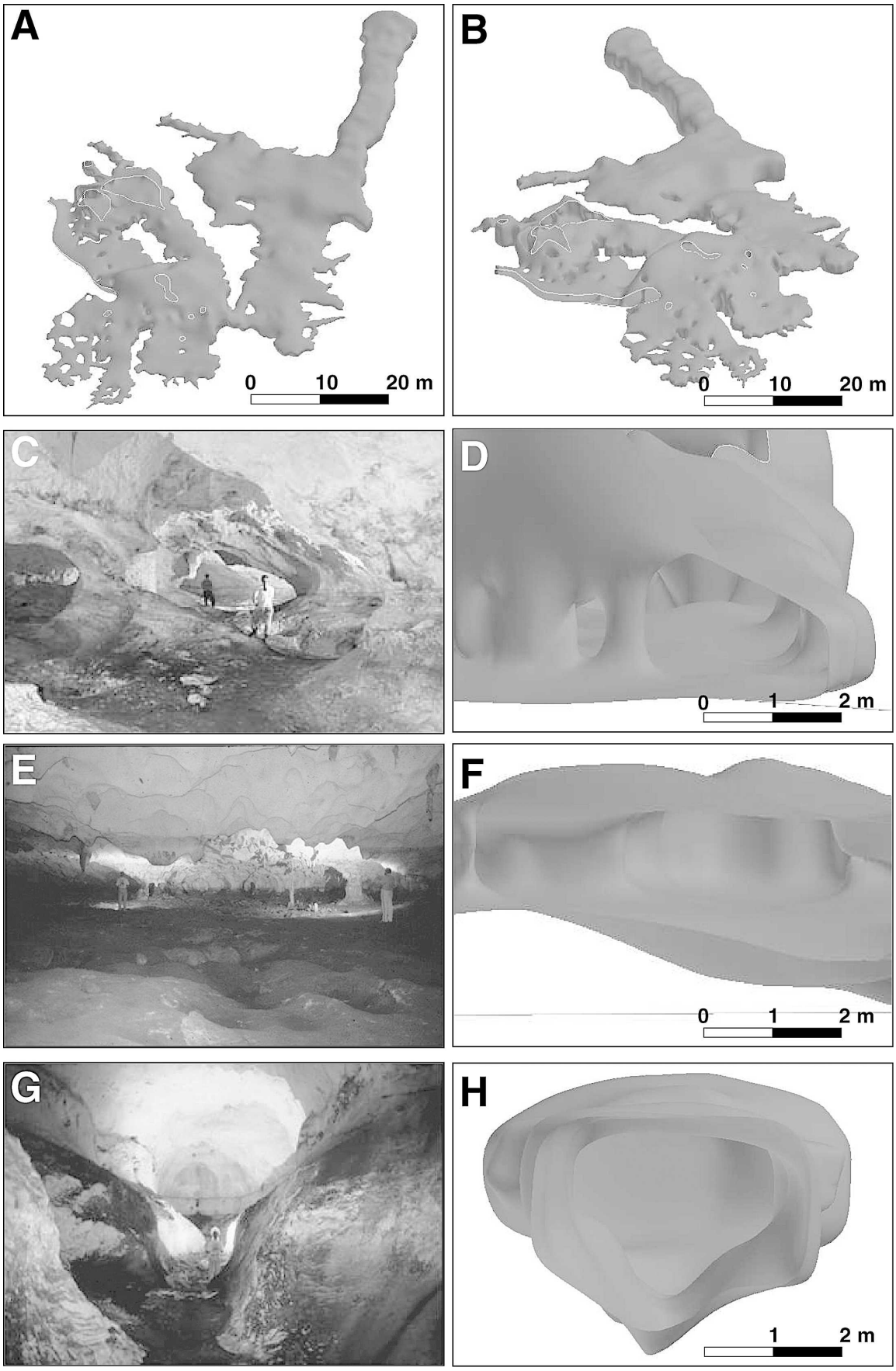
A
0 10 20 m
B
0 10 20 m
C
D
0 1 2 m
E
F
0 1 2 m
G
H
1 2 m

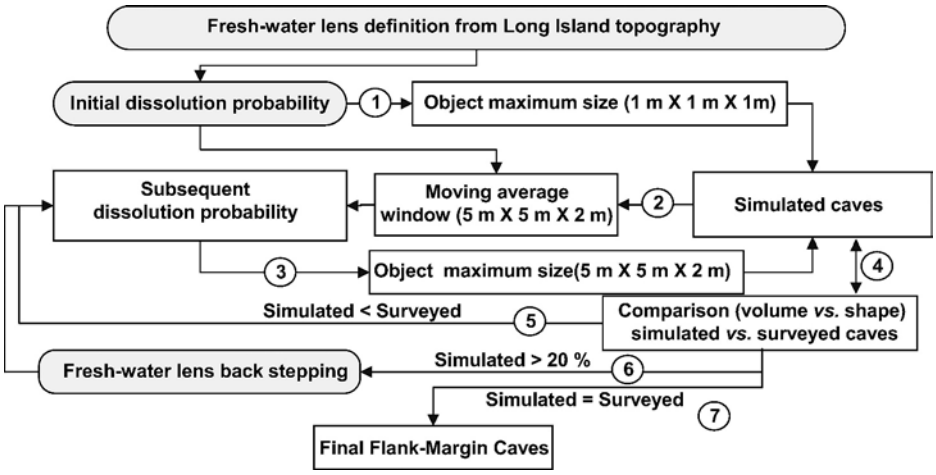

FIG. 4.—Workflow for speleogenesis of flank-margin caves. Assumption-based parts of the workflow are highlighted by gray. (1) Reconstructed fresh-water lens margin used as a basis to create a 3D probability of dissolution (maximum fixed to 0.1%). The first simulation step is performed using spherical objects of 1 m^3. (2) Simulated caves act as nuclei for subsequent simulation phases by modifying the dissolution probability using a moving-average window. (3) Subsequent simulation phases are performed using a maximum object size fixed to 5 m × 5 m × 2 m. (4) A comparison between simulated and surveyed caves (volumes and shape) is the basis for performing (or not) the next simulation phase. (5) If the simulated results have not reached observed data characteristics (shape and volume), another simulation phase is performed using the previous workflow. (6) If the created volume reaches 20% near the shoreline (that is, 20% of macroporosity), voids are assumed to be dominated by sea-water chemistry, resulting in a back-stepping of the fresh-water lens (assumption = 35 meters). The next simulation phases use the same workflow as described previously, but taking into account the new location of the fresh-water lens. (7) When simulated and surveyed caves have the same shapes and volumes, the simulation process is stopped.

FROM DETERMINISTIC REPRESENTATION TO STOCHASTIC OBJECT MODELING

The geometry of flank-margin caves is a non-constant parameter, as revealed by numerous surveyed caves in recent years (e.g., Roth 2004; Lascu 2005). In order to model cave morphologies characterized by globular chambers, the simulated objects are simple spheres. The coalescence of these spheres will reproduce the observed globular aspect of the caves. In order to condition boolean simulations, the CIKM concepts involved in formation of flank-margin caves were integrated into our model using probability cubes.

First, a fresh-water lens was constructed based on the Long Island topography in the Salt Pond Cave area. Using the carbonate-island karst model, a simple model of a homogeneous carbonate island was created, maintaining the 1:40 ratio between the height of the lens above sea level and the depth below sea level. The reconstructed fresh-water lens margin is used as a basis for development of flank-margin caves in order to create a 3D probability of occurrence of dissolution voids (Fig. 4—workflow step 1). In order to construct a variety of chamber morphologies, the simulation is performed in sequential phases (Table 1). Initially, the object size is limited to one cubic meter (cell size in modeling grid). The first simulation phase is used to generate dissolution seeds for subsequent stages of virtual cave growth. In this first stage the dissolution probability is defined as maximum at fresh-water lens margin and progressively decreases moving away from it (Fig. 5). The resulting 3D dissolution probability precisely reflects the geometry of the flank-margin cave. A dominant dissolution area is located in the seaward part of the lens (0.1%) where the mixing of waters at the bottom of the lens encounters the vadose–phreatic interface. The dissolution probability decreases landward and away from the location of the fresh-water lens. In our example, this dissolution probability is totally independent of initial sediment porosity and permeability. Nevertheless, any variations in petrophysical characteristics may generate shape complexities in the fresh-water lens, leading to preferential dissolution areas along existing sedimentary features and structural networks.

These initial simulated caves act as nuclei for the subsequent simulation phases. The dissolution probability of the second generation voids is calculated by modifying the initial probability cube (Fig. 4—workflow step 2). The second probability cube is obtained by increasing the dissolution probability around the initial simulated objects by using a "moving-average window." The moving-average window is restricted to five meters horizontally and two meters vertically, roughly the same size of the smallest surveyed caves in the Bahamas (Roth 2004). Initial simulated voids are defined as hard conditioning data for the next simulation (Fig. 6). Later simulation phases use bigger objects (Fig. 4—workflow step 3), the ellipsoidal objects being upscaled to a maximum size of five meters horizontally and two meters vertically (cf. Roth 2004; as above). During subsequent simulation phases, uncertainties in void size are introduced by defining dimension variations based on the distance from fresh-water lens margin. As for dissolution probability, the size of the simulated objects depends on the morphology of the fresh-water lens. The maximum size is located where the mixing of waters at the bottom of the lens encounters the vadose–phreatic interface and then decreases landward with distance away from fresh-water lens.

At each simulation phase a comparison between simulated and surveyed caves (volumes and shape) is performed, in order to estimate if subsequent simulation phases are needed (Fig. 4—workflow steps 4 and 5). As a result of the five simulation phases the new macroporosity is 20% at four meters from the shoreline. At this high level of macroporosity, the voids are dominated by sea-water chemistry. This would result in a change of location of the fresh water lens, mainly backstepping landward (Fig. 4—workflow step 6). To simulate this phenomenon in our modeling

←

FIG. 3.—Comparison between observed cavity and reconstructed Salt Pond Cave. **A**, **B)** 3D visualization of reconstructed Salt Pond Cave. **C**, **D)** Comparison between reconstructed and observed pillars. **E**, **F)** The globular aspect of the chambers. **G**, **H)** Comparison between reconstructed and observed phreatic tube.

TABLE 1.—*Simulation phases—summary and results. For the eight phases the summary can be seen in column B. Columns C and D show the distributions of both general (all caves) and specific statistics (ten biggest caves). Columns E, F and G, provide the simulated volumes, mean and cumulated dissolution capacity. The final column H, gives an approximate length of time.*

	A	B		C		D		E	F	G	H
	Simulation phase	Initial probability (%)		Simulated cave statistics (m^3)		Simulated cave statistics (m^3) up to rank number 10		Simulated volumes (10^3 m^3)	Mean dissolution capacity* (10^3 m^3)	Cumulated dissolution capacity (10^3 m^3)	Calculated age (yr) From the beginning of IOS 5 (divided 6.5 m^3/yr)
1st Generation	Phase 1	mean	0.01	Min	1	Min	1	0.15	0.13	0.13	20
		Max	0.10	Max	2	Max	2				
		Min	0.00	Mean	1	Mean	1				
				Std. Dev.	0	Std. Dev.	0				
	Phase 2	mean	0.24	Min	1	Min	29	1.80	1.20	1.33	200
		Max	1.69	Max	80	Max	80				
		Min	0.00	Mean	9	Mean	44				
				Std. Dev.	20	Std. Dev.	18				
	Phase 3	mean	0.27	Min	1	Min	111	4.70	9.87	11.20	1700
		Max	35.00	Max	282	Max	282				
		Min	0.00	Mean	19	Mean	184				
				Std. Dev.	34	Std. Dev.	52				
	Phase 4	mean	0.53	Min	1	Min	327	16.70	14.60	25.80	4000
		Max	64.00	Max	2636	Max	2636				
		Min	0.00	Mean	64	Mean	1155				
				Std. Dev.	235	Std. Dev.	801				
	Phase 5	mean	1.44	Min	1	Min	517	22.00	17.34	43.14	6600
		Max	87.00	Max	4664	Max	4664				
		Min	0.00	Mean	137	Mean	2430				
				Std. Dev.	526	Std. Dev.	1542				
2nd Generation	Simulation phase	Initial probability(%)		Simulated cave statistics (m^3)		Simulated cave statistics (m^3) up to rank number 10		Simulated volumes(10^3 m^3)	Mean dissolution capacity* (10^3 m^3)	Cumulated dissolution capacity (10^3 m^3)	Calculated age (yr) From the beginning of IOS 5 (divided 6.5 m^3/yr)
Backstepping of the fresh-water lens	Phase 1	mean	0.38	Min	1	Min	672	8.00	15.00	58.14	8900
		Max	77.00	Max	4664	Max	4664				
		Min	0.00	Mean	116	Mean	2491				
				Std. Dev.	471	Std. Dev.	1534				
	Phase 2	mean	0.95	Min	1	Min	976	10.20	2.09	60.23	9200
		Max	91.00	Max	4664	Max	4664				
		Min	0.00	Mean	105	Mean	2672				
				Std. Dev.	434	Std. Dev.	1464				
	Phase 3	mean	2.06	Min	1	Min	1010	14.80	17.94	78.17	12000
		Max	95.00	Max	4776	Max	4776				
		Min	0.00	Mean	129	Mean	2874				
				Std. Dev.	515	Std. Dev.	1433				

* Mean dissolution capacity (m^3) = mean probabilty * mean object dimension (calculated in all cells) − previous simulated volume (m^3)
Yearly dissolution rate = 78170 (m^3)/12 000 (years) = 6.5 (m^3/yr)
Yearly dissolution rate per km^2 = 6.5 (m^3/yr)/Fresh-water lens area: 81.10^{-3}(km^2) = 80 (m^3/km^2/yr)

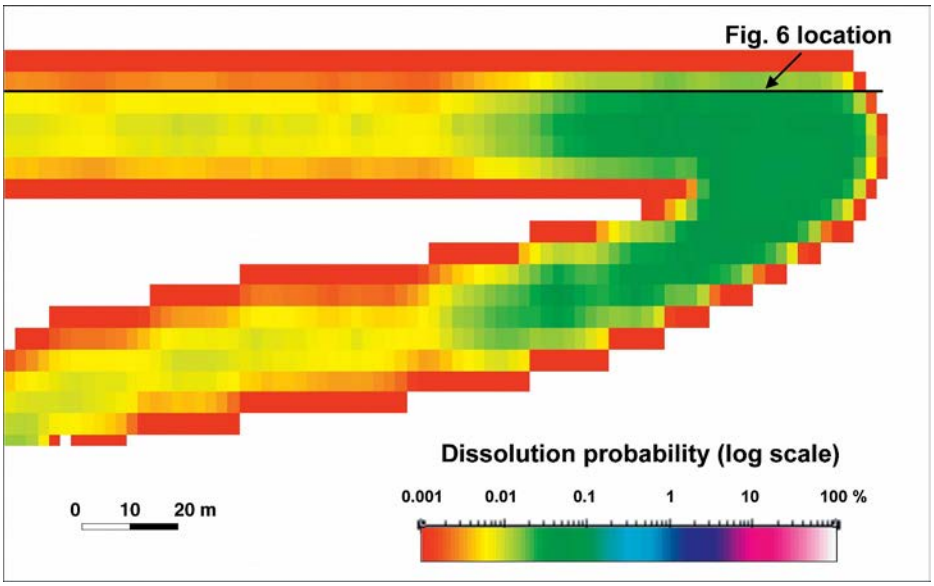

FIG. 5.—Dissolution probability in the reconstructed fresh-water lens margin. Dissolution probability in the first stage is defined as maximum at the fresh-water lens margin and decreases progressively away from it. The resulting 3D dissolution probability reflects the geometry of the fresh-water lens, with a dominant dissolution area located in the seaward part of the lens (maximum probability: 0.1%).

workflow, the lens position is shifted horizontally 35 meters inland. The original caves intersected by the new fresh-water lens are used as seeds for the second generation of caves. Three phases of cave growth were performed incorporating the new lens position and using the same procedure described above. When simulated and surveyed caves show nearby shapes and volumes, the simulations process is assumed to be completed (Fig. 4—workflow step 7).

Table 1 shows the evolution of input parameters (column B), throughout the successive simulation phases, and associated results (columns C to F). Only first-simulation-phase initial parameters are defined; the other initial probabilities are derived from the previous simulations.

DATA ANALYSIS

The computer-generated caves closely reproduce the morphology of flank-margin caves. Similarities between the virtual caves and the mapped caves include shape, size, relation with neighboring voids, as well as distance from island coast (Fig. 7). The spherical shape of the original object enables the globular morphology of the chambers to be accurately reconstructed. This resulting morphology shows pillars in large-scale caves, connections between different chambers highlighting the effect of the fresh-water lens backstepping, and also the intersection of neighboring voids (Fig. 8). The small cell size (one cubic meter) and the coarse grid (4.7×10^6 cubic meters) allows us to generate large caves as well as detailed morphologic patterns.

To make the comparisons between virtual caves with real caves, a database of simulated cave parameters (perimeter, area, area rank number) was created and then compared with the Bahamian flank-margin cave 2D database (Roth 2004). The area and perimeter of each simulated cave were calculated by projecting the three-dimensional reconstruction onto a horizontal plane. Simulated cave areas range from 1 m^2 to 1685 m^2, and the perimeters range from 4 m to 540 m. Of the 190 simulated flank-margin caves, 143 caves have an area less than 100 m^2, 41 caves have an area of between 100 m^2 and 1000 m^2, and 5 caves have an area greater than 1000 m^2. Very large caves (with an area $>$ 2000 m^2) could not be simulated because of the limited size of the modeled area.

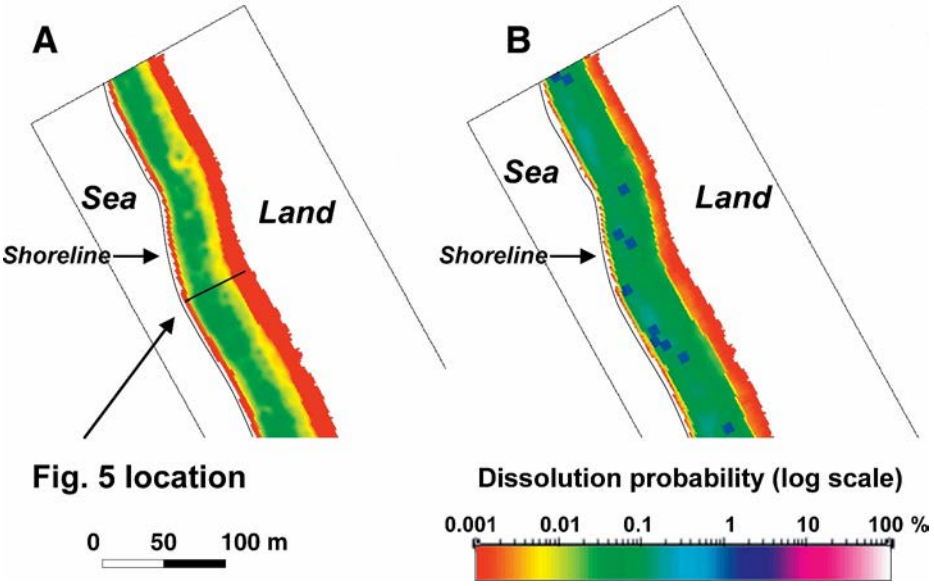

FIG. 6.—**A)** Initial dissolution probability. **B)** The second probability cube is obtained by increasing the dissolution probability around initial simulated objects by using a moving-average window. The moving-average window is restricted to five meters horizontally and two meters vertically.

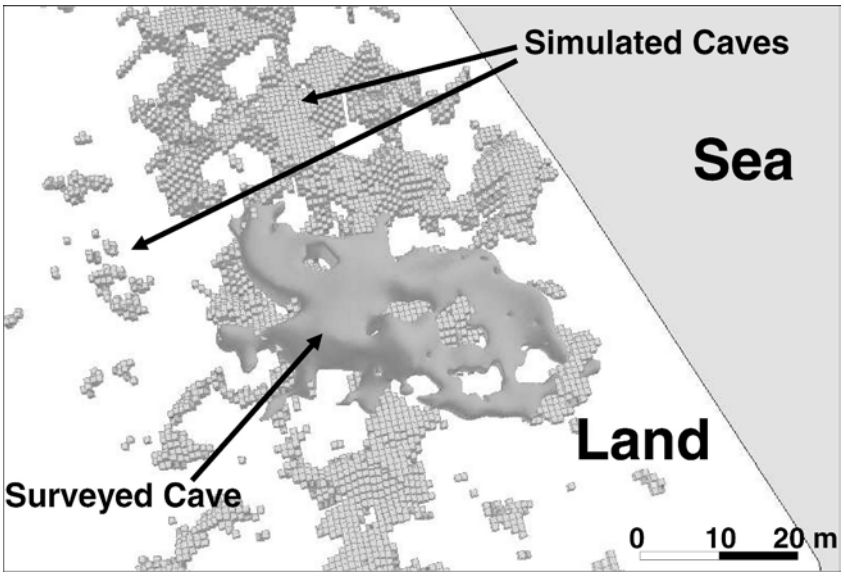

FIG. 7.—Comparison between virtual caves and real flank-margin caves. Strong similarities can be seen in complex morphologic developments. Both consist of large central chambers, with maze-like passages developing toward the interior of the ridge containing the chambers. Inland, rarely mapped small caves are simulated.

However, all other virtual cave dimensions (perimeter and area) are comparable with those surveyed.

In addition to the Bahamian flank-margin cave database, a smaller cave class appeared among the simulated caves, 61 caves with an area less than 14 m^2 (smallest surveyed cave in the Bahamas database). These very small caves are mainly developed inland (Fig. 7), and undergo little if any erosive exposure. This additional class of data points concerns only very small caves, which are rarely mapped, even when found in the field (White 1988). Cave area plotted against cave perimeter in Figure 9 shows a similar distribution of simulated and surveyed caves, but with a wider dispersal for surveyed caves. This heteroscedasticity (a sequence of random variables with different variances) observed in the distribution of surveyed *versus* simulated caves is probably linked to variations of initial sediment permeability that where not taken into account in our modeling workflow.

Ranking flank-margin caves by size and plotting them against their areas shows an exponential relationship for both surveyed and simulated caves (Fig. 10). This relationship can be explained by small voids which are linked together nonlinearly to form larger voids. The sudden increase in size is associated with coalescence.

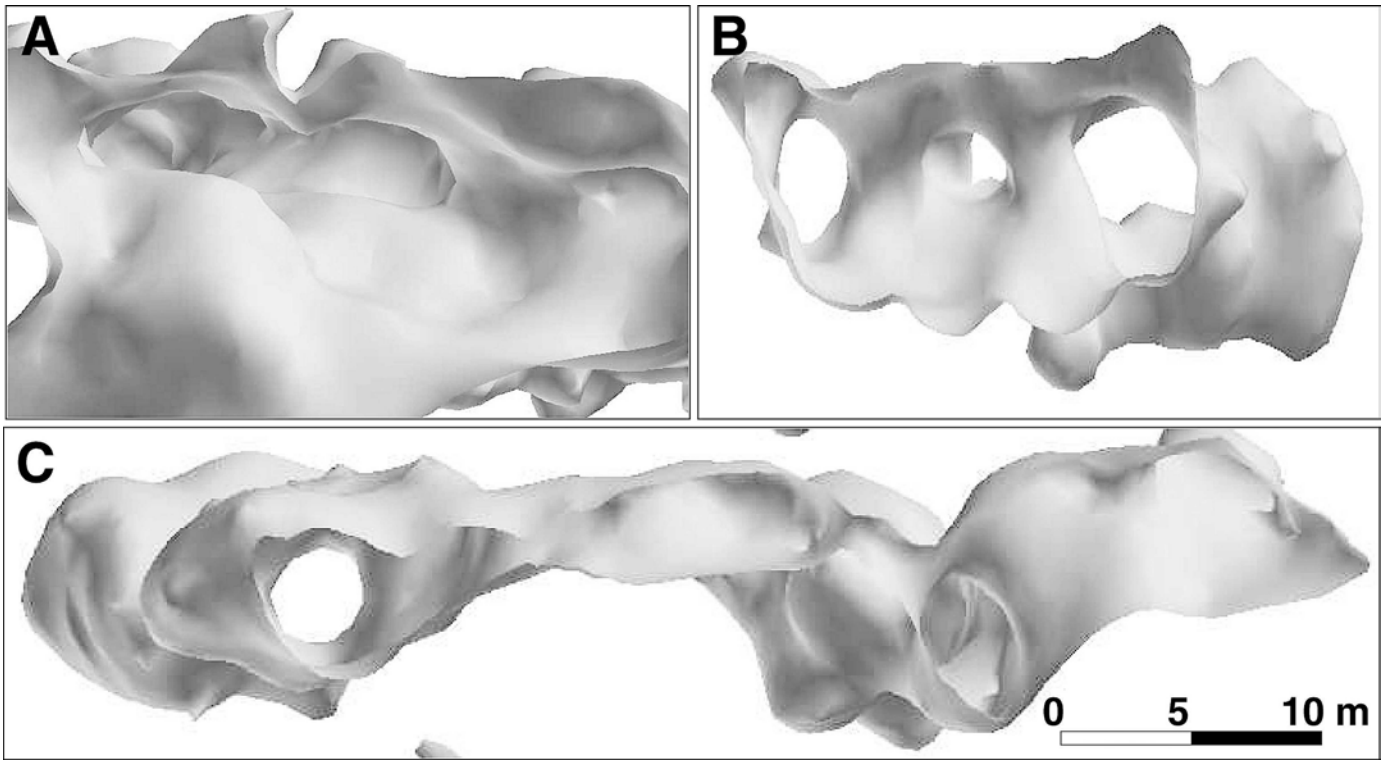

FIG. 8.—Typical simulated morphology: **A)** globular chambers, **B)** pillars in larger caves, **C)** interconnecting passages between chambers (cf. Fig. 3—Salt Pond Cave reconstruction).

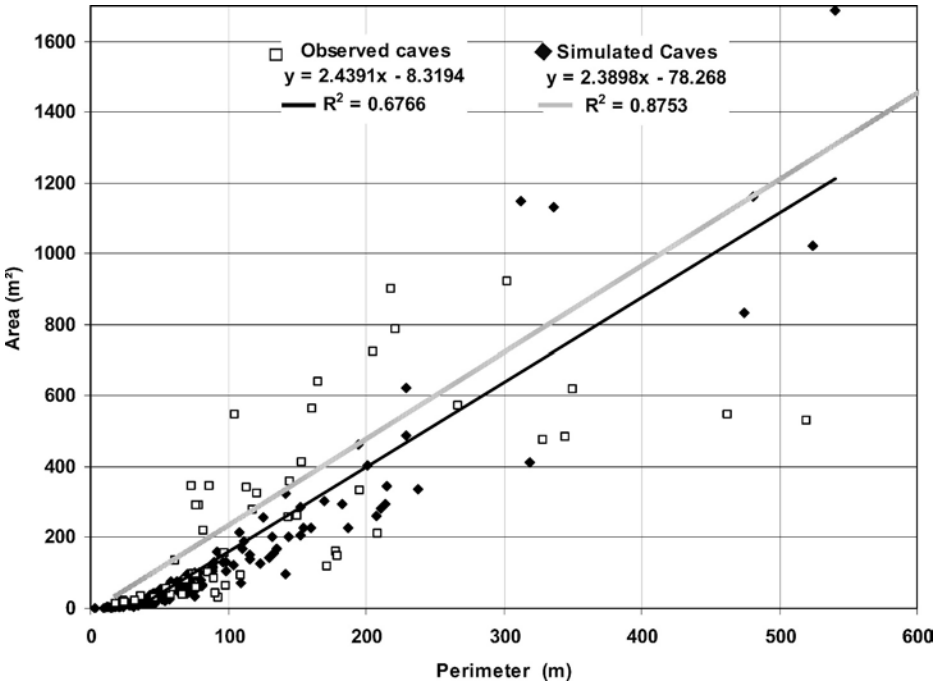

FIG. 9.—Area plotted against perimeter for surveyed and simulated flank-margin caves. There is a significantly higher frequency of small and medium sized caves than large caves. The heteroscedasticity in the distribution of surveyed versus simulated caves can be explained by host-rock initial permeabilities not taken into account in our modeling workflow.

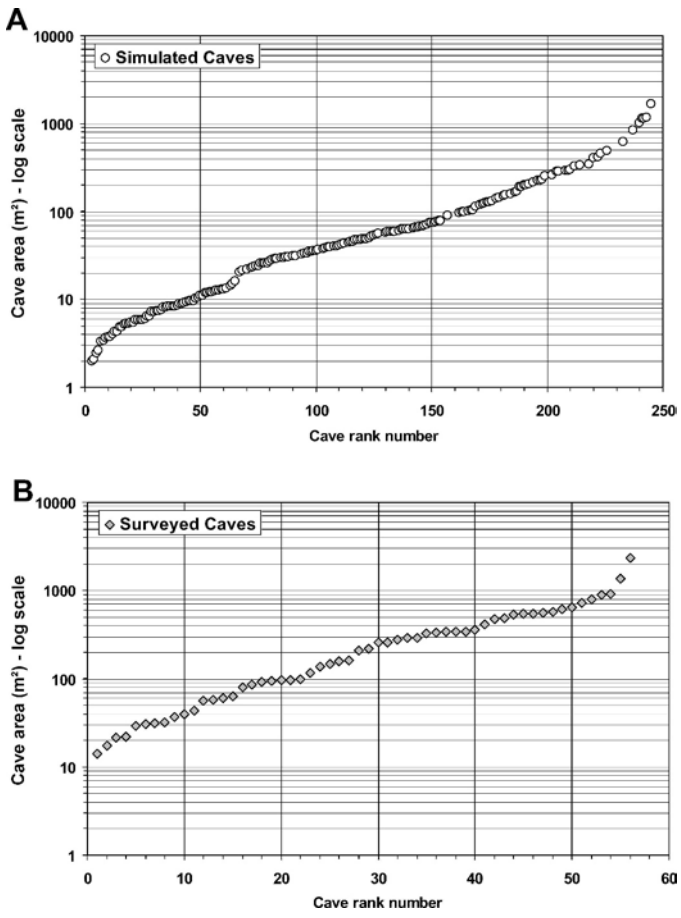

FIG. 10.—Area (log scale) plotted against rank number applied to **A)** simulated caves and compared with **B)** surveyed Bahamian caves (Roth 2004). A nonlinear (exponential) relationship can be observed for surveyed and simulated caves. The coalescence of smaller voids results in larger voids formed nonlinearly.

Table 1 summarizes the results of the different dissolution phases; simulated cave statistics (column C) shows the production of small-size caves (< 5 m^3) at each step of the modeling workflow. The mean cave dimension increases throughout the modeling steps up to the backstepping of the fresh-water lens when the mean decreases and small caves form behind earlier ones. The same statistics applied to the biggest generated caves (column D) show a constant increase of the mean volume of simulated caves even after the backstepping of the fresh-water lens. This underlines the coalescence generated by such a landward movement on the biggest caves despite a strong reduction in carbonate removal (Table 1).

DISCUSSION ON SPELEOGENESIS OF FLANK-MARGIN CAVES

The main uncertainty of our modeling workflow lies in the initial 3D dissolution probability. The numerous surveyed caves along Bahamian shorelines do not reflect the true density of flank-margin caves because of many unobservable caves. Because the initial dissolution probability is the driving parameter for subsequent simulations (later modeling phases are derived and conditioned by this initial probability), several sensitivity tests were carried out. In normal circumstances the numerous resulting models would have been sorted according to the distribution of simulated caves, by using field data (well or production data). In our case, however, because no relevant data were available this sorting was defined using the veracity of the produced image as the criterion. The best results were obtained using a maximum dissolution probability of 0.1%. Object-based stochastic models enable us to define an uncertainty coefficient on the initial probability and therefore to incorporate uncertainty related to lens position and stability time.

During the last interglacial period or Oxygen Isotope Stage (OIS) 5e, some 125 ka ago, sea level was 6 m above present for 12,000 years (Chen et al. 1991; Muhs 2002). If we assume a constant dissolution rate through time, we can calculate a mean dissolution rate for each modeling phase taken from the dissolution probability and the mean object size applied to each cell of the model (Table 1, columns F and G). Our simulation reaches a carbonate removal rate of 6.5 m^3/year. According to the aforementioned assumption, we can estimate the duration of each simulation phase (Table 1, column H), which led to a backstepping of

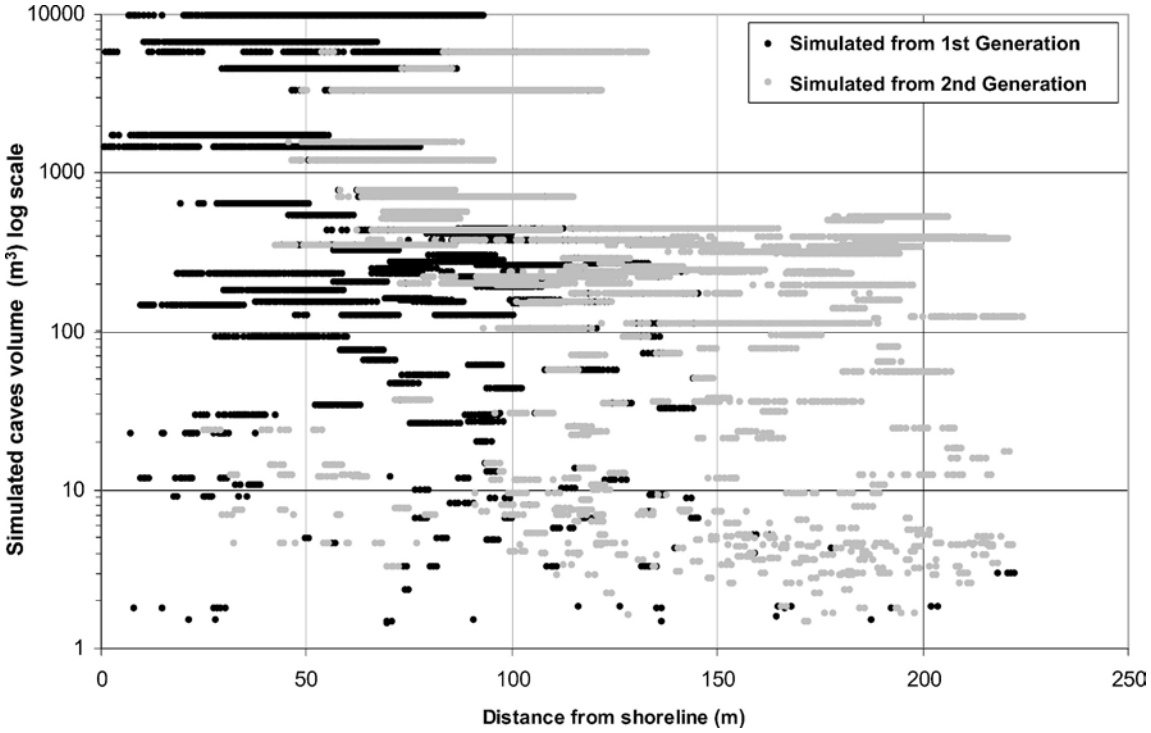

FIG. 11.—Simulated cave volumes (log scale) plotted against distance from original shoreline. The distribution shows the largest caves at around 10 to 100 meters from shoreline. Medium caves are located between 30 to 230 meters from shoreline. Dissolution resulting from the first (black dots) and the second (gray dots) workflow generations highlights the influence of backstepping of the fresh-water lens on cave size distribution.

the fresh-water lens approximately 6,600 years after OIS5e sea-level stage began. Each simulation phase produces not only expansion of individual caves but also linking of neighboring voids. The second and third phases of the simulation result in the formation of small caves (1,700 years after OIS5e began). The fourth and fifth phases illustrate the development of medium to large caves (6,600 years after OIS5e began).

In Figure 11 we can observe the distribution of simulated caves related to the distance from original shoreline. This figure shows the impact of the second cave generation (after fresh-water lens backstepping) on the distribution of simulated caves. The backstepping of the fresh-water lens allowed a second row of chambers to be generated, and in certain places, to be connected with the first row of chambers, resulting in the generation of larger caves. The simulations demonstrate that, often, only a small connection (one cell of the grid) is necessary to provide the link-up between adjacent voids, resulting in an exponential relationship between cave sizes.

The rate of global carbonate removal derived from the simulation is 80 m^3/km^2/year. This result is close to the average yearly rate of carbonate removal of 77.56 m^3/km^2 calculated for large Bahamian flank-margin caves (Lascu 2005). The spatial and visual similarity between simulated and surveyed flank-margin caves suggests that both the initial simulation parameters and the resulting simulations are close to reality.

COLLAPSE AND SIDE EFFECTS

Collapse and side effects were studied from two perspectives: first, as an early collapse effect, as seen in the Bahamas and Bermuda (Fig. 12—workflow step 1), and second, as a burial effect on collapsed cave deposits, following the observations and concepts developed by Loucks (1999b), but in this case applied to an eogenetic environment (Fig. 12—workflow step 2). Early collapse was based on the assumption that if

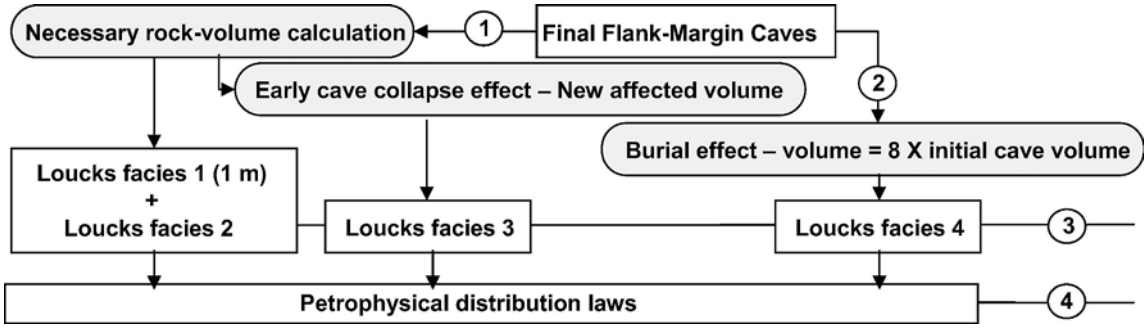

FIG. 12.—Collapse and burial modeling workflow. (1) Deterministic calculation of early collapse effect (two and a half times initial cave volume). (2) Deterministic calculation of burial-effect volume (eight times initial cave volume). (3) The different generated volumes are filled respectively with facies from Loucks classification. (4) Simulation of the petrophysical characteristics for each Loucks facies.

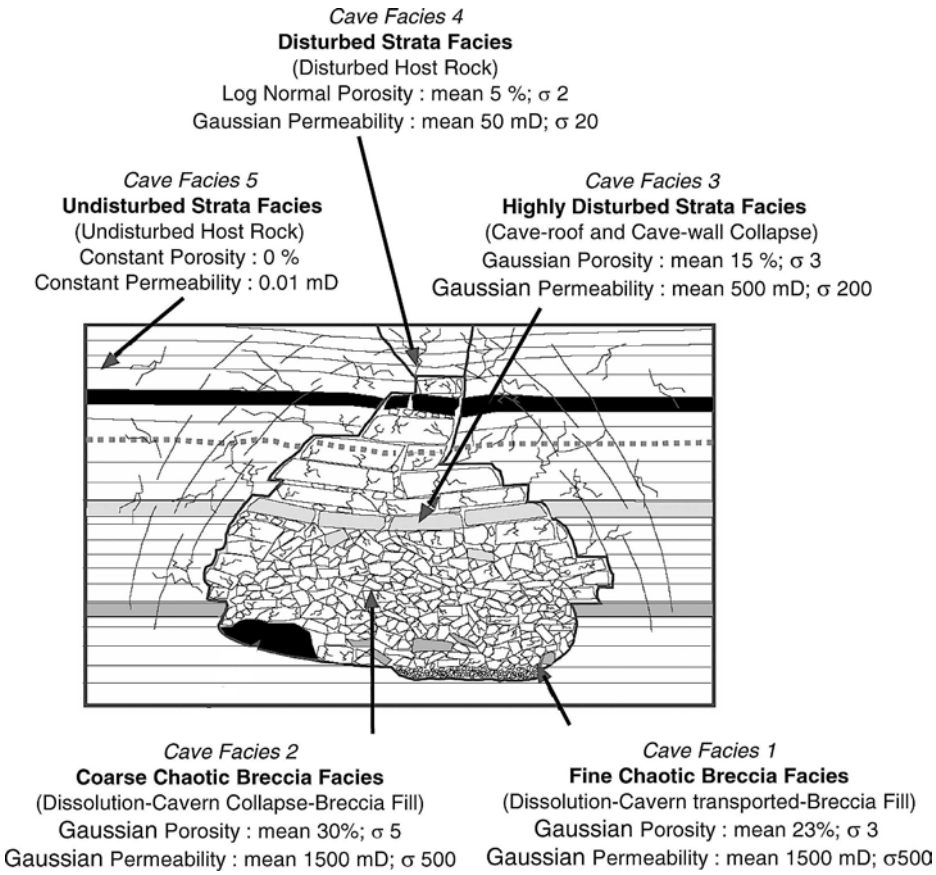

FIG. 13.—Composite diagram displaying the cross section of a collapse paleocave passage with the classification of paleocave facies and their distributions of petrophysical parameters (modified from Loucks and Mescher 2001).

a solid block of rock is turned into breccia, its volume increases by 40%. This means that, for a void with a volume of 1 unit a rock volume of 2.5 units is needed to occupy both the void volume and its initial volume when brecciated. The simulated caves are assumed to be filled by any overlying available material (Fig. 12—workflow step 1). Obviously, if the available rock volume is less than 2.5 times the cave volume, the material will not entirely fill the void, resulting in a negative topographic expression (a collapse sinkhole). This morphology can be compared with that of a banana hole (Mylroie et al. 1991; Harris et al. 1995).

Later burial effects are more complex and include the homogenization of chaotic breccias and cave-sediment fill from passages, chambers, and shafts as well as crackle breccia from pillars, roof rock, and wall rock (Mescher 1996). Cave systems continuously undergo extensive mechanical compaction and collapse from soon after their formation and right until their burial (Loucks and Handford 1992). This affects not only passages and chambers, but also the host rock in the walls, pillars, and overlying roof. As the cave system is buried into the deeper subsurface, wall and roof strata surrounding open passages collapse and form breakdown breccias (McMechan et al. 1998). As shown by Loucks (1999b), subsequent burial increases the affected rock volume eight times the initial cave volume. Loucks and Mescher (2001) have developed a classification of paleocave facies describing this collapsed infill volume (Fig. 12—workflow step 2 and Fig. 13). Five basic cave facies are recognized in a paleocave system and are classified by rock texture, fabric, and structure:

1. fine chaotic breccia (transported-breccia cavern fill),
2. coarse chaotic breccia (collapsed-breccia cavern fill),
3. highly disturbed strata (collapsed roof and wall rock),
4. disturbed strata (disturbed host rock),
5. undisturbed strata (undisturbed host rock).

Applying Loucks' (1999b) equations a burial effect is introduced into our model, and the resulting volume is filled according to the Loucks and Mescher (2001) classification (Fig. 12—workflow step 3). The workflow applied is linked to both early collapse phase and additional burial effect (Fig. 14). The initial cave volume is firstly assumed to be filled by one meter of fine chaotic breccia facies (Louck facies 1). The remaining volume of initial caves is then filled with coarse chaotic breccia facies issued from roof collapse (Loucks facies 2). The early collapse volume extracted from the first collapse modeling phase is assumed to be filled by highly disturbed strata facies (Loucks facies 3). The final facies is assumed to occupy the volume around collapsed caves (Loucks facies 4) until the global volume affected has reached eight times the initial cave volume. Finally, each facies is filled with permeability and porosity using Gaussian simulations according to property distributions (Fig. 12—workflow step 4 and Fig. 14) defined by Loucks et al. (2004).

These collapses and burials have a major impact on connectivity between neighboring flank-margin caves (Fig. 15). By computing the connected volumes, before and after collapse and burial phases, we can observe the impact of the different collapse effects. Initial cave collapse leads to an increase of connected volumes, but without any impact on cave area. The connection being mainly vertical, individual caves located at the base and at the top of the fresh-water lens may then be connected by this simple collapse phase. Burial effect has a greater impact on connected volumes; the size of affected areas is extended both horizontally and vertically by disturbed strata. These new breccias and fractures radiate outwards from the collapsed cave and may intersect fractures and breccias from other collapsed passages within the system. The result is the interconnection or coalescence of cave-passage chaotic breccias by crackle and mosaic breccias and fractures.

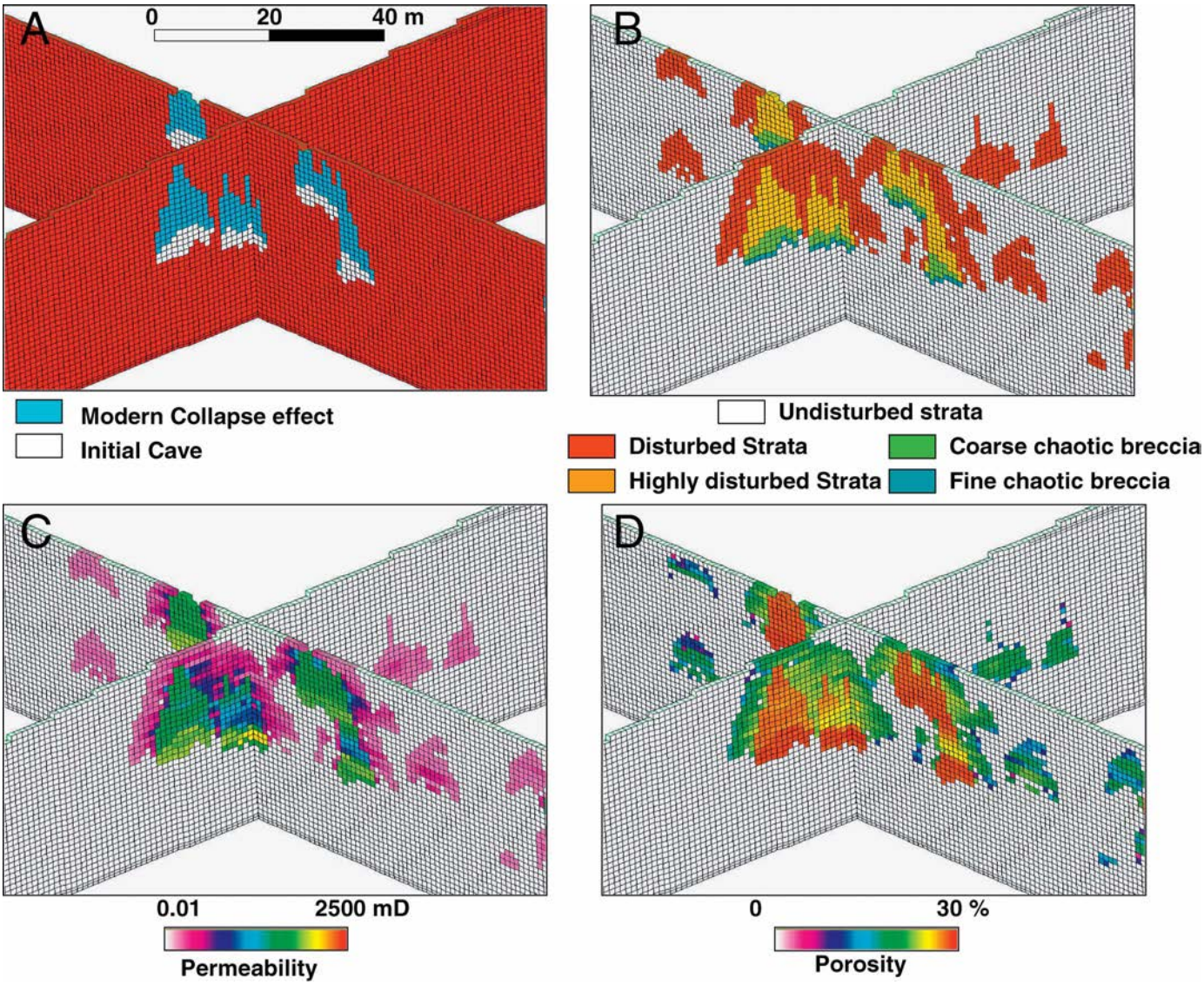

FIG. 14.—Workflow of burial effect applied to simulated flank-margin caves. **A)** Initial cave locations (white) and their associated early collapse effect (light blue). **B)** Burial effect on collapse distribution and its associated cave facies (Loucks classification 1999b). Initial cave volume is filled with one meter of fine chaotic breccia facies (dark green), and coarse chaotic breccia facies (light green). The early-collapse volume is filled with highly disturbed strata facies (orange). Disturbed strata facies occupy the remaining volume around collapsed caves (red) until the global volume affected is eight times initial cave volume. **C)** Example of derived permeability distribution. **D)** Example of derived porosity distribution.

The resulting model can be used to estimate the probability of occurrence of connected volumes according to the distance from the original shoreline. Figure 16 compares the distribution of the different classes of simulated caves (caves, early collapse, and burial effect) according to their distance from the original shoreline. This figure shows two distinct areas of increase in cave probability. The first is located near the shoreline and reflects the position of the fresh-water lens. The second, 150 meters inland, reflects the backstepping of the fresh-water lens. This distribution can be used as a guide to generate reservoir models in coherence with the maturity of the flank-margin cave network. The coalescence of a cave system into larger, connected-porosity zones results in a heterogeneous reservoir of several hundred meters in width. The probability of encountering buried connected volumes depends on the distance from the original shoreline. At 40 meters, with only 3% occurrence of original caves, the probability is 9% to 10%. At around 150 meters, with 1% occurrence of original caves, the probability is 5% to 6%. This burial coalescence consequently forms a much larger exploration target than that resulting from the collapse of a single cave passage (McMechan et al. 1998).

CONCLUSIONS

The methodology for modeling flank-margin caves and associated burial collapse effects is based on well-documented concepts and greatly increases the chances of predicting reservoir position, shape, and characteristics in preserved margin karst systems. In the case of burial preservation of island karst or continental-margin karst, their reservoir impact is more predictable than in non-margin settings, due to their precise location at the periphery of carbonate platforms.

The modeling workflow allows the reconstruction of both geometry and dimensions of flank-margin caves. It is consistent with the initial assumptions and cave generation hypothesis in its reconstruction of the

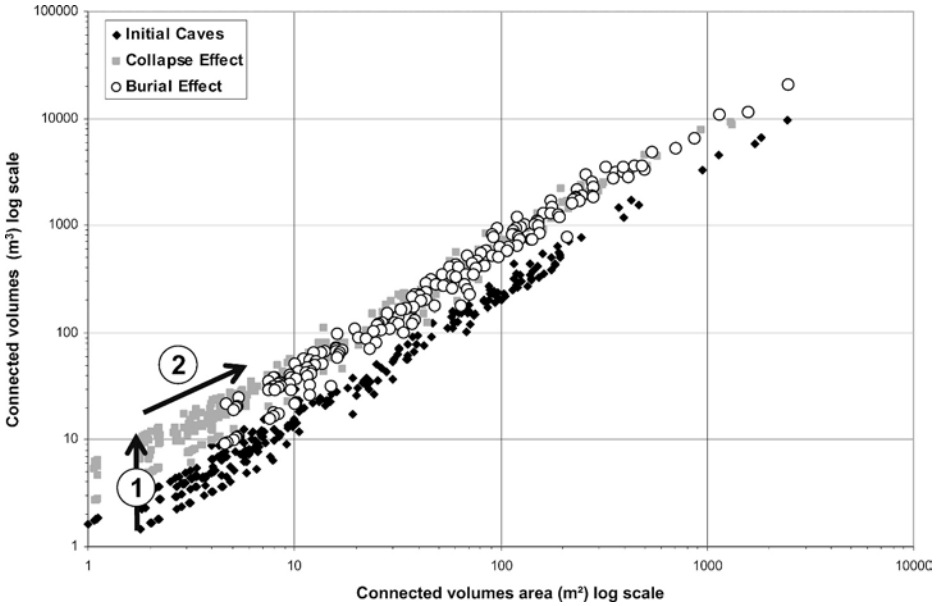

FIG. 15.—Connected volume (log scale) plotted against area of connected volumes (log scale), showing the evolution of connectivity throughout the different collapse phases. (1) Early collapse effect increases the connected volumes without any impact on area (vertical connectivity) whereas burial effect (2) increases both area and connected volumes.

observed morphologies and cave densities. The connection between different cave generations, created by an inland shift of the fresh-water lens, seems to be a reliable explanation for Bahamian cave speleogenesis. Large flank-margin caves form as the result of the intersection of small and medium-sized flank-margin caves. The main uncertainty is the relation between fresh-water lens stability time and dissolution probability. Up to now our modeling workflow is incapable of resolving this uncertainty; it is able to approach the uncertainty only by applying coefficients and comparing the final morphologies and size of simulated caves with surveyed ones. This inability underlines the fact that process-based models are needed in order to adequately explore hypotheses and to produce and test concepts, which can be incorporated in ''process-like'' workflows, as described in this paper.

Burial collapse effects were applied deterministically to the above results, using criteria developed by Loucks (1999a), to hypogenic karst. This artificial collapse stage allows imaging of the possible spatial and petrophysical impact of a buried flank-margin cave analog. The results show an increase in connected volumes leading to a complex reservoir architecture closely linked to the initial dissolution area.

Paleocave reservoirs have a complex formation background. These reservoirs are products of near-surface cave development, including dissolution excavation, breakdown, and cave sedimentation. The resulting near-surface cave systems are three-dimensional megapore networks containing varying amounts of breccias and sediments.

Contrary to process-based models, this workflow enables access to multiple distributions of paleocave reservoir characteristics without any complex parameter definition (water characteristics, dissolution potential of host rocks, etc.). This model is both stochastic and deterministic in that it generates dissolution voids with equal probability of appearance. However, our modeling workflow is driven by probability cubes, defining constraints of location as well as horizontal and vertical expansions. The resulting parameters (shape, distribution, statistical repartition) can also

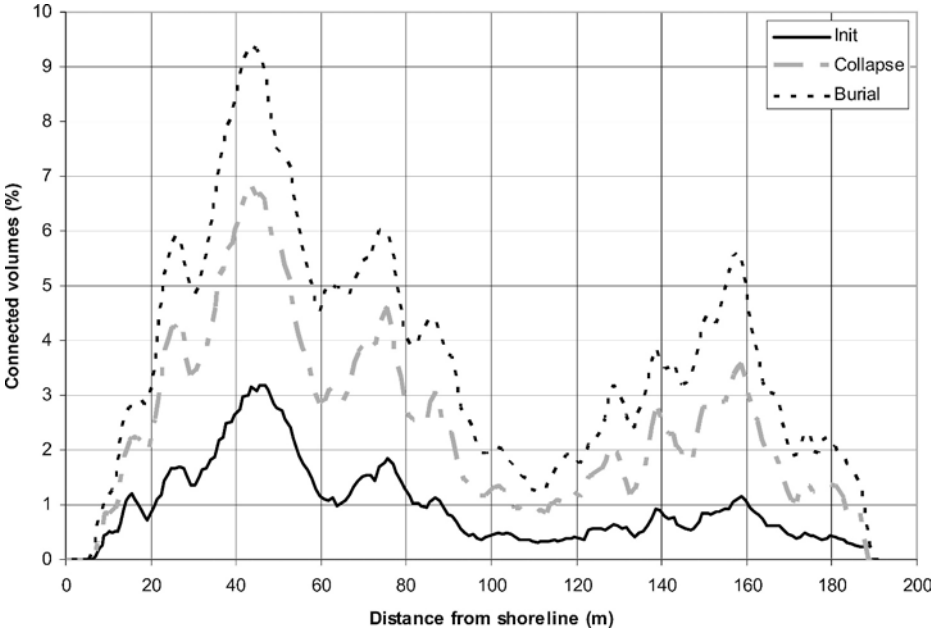

FIG. 16.—Occurrence of connected volume plotted against distance from original shoreline. Two distinct areas of cave probability rise can be distinguished. The first is located near the shoreline (20 to 60 meters), reflecting the initial position of the fresh-water lens. The second, 150 meters inland in accordance with backstepping of the fresh-water lens.

be used to simulate real hydrocarbon reservoirs using classical geostatistic simulations or to generate training images for multipoint geostatistics.

This study shows that it is possible to derive simple object simulations with deterministic laws, allowing the reconstruction of reliable geobodies. It can be applied and modified to assess different types of diagenetic overprints. As soon as a process is known and its final product can be imaged, deterministic methods coupled with stochastic simulations can generate optimum models.

ACKNOWLEDGMENTS

The authors thank Herbert Eishenseer and Bernard Geiss, who initiated this project and involved us in it, and Wolfgang Dreybrodt for discussions on concepts relating to the evolution of island karst. The authors would also like to thank Eugene Rankey, Kitty Milliken, Robert Loucks, Sean Guidry, Donald McNeill, Sandra McJannett, and two anonymous reviewers, who offered many useful and constructive comments that helped improve the manuscript. The authors thank Chris Beck, Beth Fratesi, Mike Lace, PJ Moore, Marc Ohms, Rene Ohms, Kali Pace-Graczyk, and Kevin Toepke for the detailed survey of Salt Pond Cave. The authors thank Total for permission to publish this article.

REFERENCES

Beach, D.K., and Ginsburg, R.N., 1980, Facies succession of Pliocene–Pleistocene carbonates, northwestern Great Bahama Bank: American Association of Petroleum Geologists, Bulletin, v. 64, p. 1634–1642.

Bögli, A., 1980. Karst Hydrology and Physical Speleology: Berlin, Springer-Verlag, 270 p.

Bottrell, S.H., Carew, J.L., and Mylroie, J.E., 1993, Bacterial sulfate reduction in flank margin environments: Evidence from sulfur isotopes, *in* White, B., ed., Proceedings of the Sixth Symposium on the Geology of the Bahamas: San Salvador, Bahamas, Bahamian Field Station, p. 17–21.

Briggs, R.P., and Seiders, V.M., 1972, Geologic map of Isla de Mona quadrangle, Puerto Rico: U.S. Geological Survey. Miscellaneous Investigations, Map I-718.

Candelaria, M.P., and Reed, C.L., 1992, Paleokarst related diagenesis and reservoir development: examples from Ordovician–Devonian age strata of West Texas and the Mid-Continent: SEPM, Permian Basin Section, 1992 Annual Field Trip, Franklin Mtns., El Paso, Texas, April 9–11, 202 p.

Carew, J.L., and Mylroie, J.E., 1995, Quaternary tectonic stability of the Bahamian Archipelago: Evidence from fossil coral reefs and flank margin caves: Quaternary Science Reviews, v. 14, p. 145–153.

Chen, J.H., Curran, H.A., White, B., and Wasserburg, G.J., 1991, Precise chronology of the last interglacial period: $_{234}U-_{230}Th$ data from fossil coral reefs in the Bahamas: Geological Society of America Bulletin, v. 103, p. 82–97.

Craig, D.H., 1988, Caves and other features of Permian karst in San Andres Dolomite, Yates Field Reservoir, West Texas, *in* James, N.P., and Choquette, P.W., eds., Paleokarst: New York, Springer-Verlag, 416 p.

Dreybrodt, W., 2000, Equilibrium chemistry of karst water in limestone terranes, *in* Klimchouk, A.B., Ford, D.C., Palmer, A.N., and Dreybrodt, W., eds., Speleogenesis—Evolution of Karst Aquifers: Huntsville, Alabama, National Speleological Society, p. 126–135.

Ford, D.C., 1995, Paleokarst as a target for modern karstification: Carbonates and Evaporites, v. 10, p. 138–147.

Frank, E.F., Mylroie, J.E., Troester, J.W., Alexander, E.C., and Carew, J.L., 1998, Karst development and speleogenesis, Isla de Mona, Puerto Rico: Journal of Cave and Karst Studies, v. 60, p. 73–83.

Harris, J.G., Mylroie, J.E., and Carew, J.L., 1995, Banana holes: unique karst features of the Bahamas: Carbonates and Evaporites, v. 10, p. 215–224.

Holtz, M.H., and Kerans, C., 1992, Characterization and classification of West Texas Ellenburger reservoirs, *in* Candelaria, M.P., and Reed, C.L., eds., Paleokarst Related Diagenesis and Reservoir Development: Examples from Ordovician–Devonian Age Strata of West Texas and the Mid-Continent: SEPM, Permian Basin Section, 1992 Annual Field Trip, Franklin Mountains, El Paso, Texas, April 9–11, p. 45–54.

Hu, L.Y., 2003, History matching of object-based stochastic reservoirs models: Society of Petroleum Engineers, 13th Middle East Oil Show & Conference, SPE no. 81503.

Jackson, J.A., 1987. *in* Bates, R.L., ed., Glossary of Geology, 4th Edition: American Geological Institute, 769 p.

Jenson, J.W., Keel, T.M., Mylroie, J.R., Mylroie, J.E., Stafford, K.W., Taborosi, D., and Wexel, C., 2006, Karst of the Mariana Islands: The interaction of tectonics, glacioeustasy and fresh-water/sea-water mixing in island carbonates, *in* Harmon, R.S., and Wicks, C., eds., Perspectives on Karst Geomorphology, Hydrology, and Chemistry—A Tribute Volume to Derek C. Ford and William B. White: Geological Society of America, Special Paper 404, p. 129–138.

Kerans, C., 1988, Karst-controlled reservoir heterogeneity in Ellenburger Group carbonates of West Texas: American Association of Petroleum Geologists, Bulletin, v. 72, p. 1160–1183.

Lascu, I., 2005, Speleogenesis of large flank margin caves of the Bahamas [unpublished M. Sc. thesis]: Mississippi State University, 214 p.

Loucks, R.G., 1999a, Origin and attributes of paleocave carbonate reservoirs, *in* Palmer, A.N., Palmer, M.V., and Sasowsky, I.D., eds., Karst Modeling, Karst Waters Institute Special Publication no. 5, p. 59–64.

Loucks, R.G., 1999b, Paleocave carbonate reservoirs; origins, burial-depth modifications, spatial complexity, and reservoir implications: American Association of Petroleum Geologists, Bulletin, v. 83, p. 1795–1834.

Loucks, R.G., and Anderson, J.H., 1985, Depositional facies, diagenetic terranes, and porosity development in Lower Ordovician Ellenburger Dolomite, Puckett Field, West Texas, *in* Roehl, P.O., and Choquette, P.W., eds., Carbonate Petroleum Reservoirs: Berlin, Springer-Verlag, p. 19–38.

Loucks, R.G., and Handford, C.R., 1992, Origin and recognition of fractures, breccias and sediment fills in paleocave-reservoir networks, *in* Candelaria, M.P., and Reed, C.L., eds., Paleokarst Related Diagenesis and Reservoir Development: Examples from Ordovician–Devonian Age Strata of West Texas and the Mid-Continent: SEPM, Permian Basin Section, Annual Field Trip, Franklin Mtns., El Paso, Texas, April 9–11, p. 31–44.

Loucks, R.G., and Mescher, P.K., 1996, Architecture of collapsed-paleocave reservoirs: American Association of Petroleum Geologists, Annual Convention, Official Program.

Loucks, R.G., and Mescher, P.K., 2001, Paleocave facies classification and associated pore types (abstract): American Association of Petroleum Geologists, Southwest Section, Annual Meeting, 18 p.

Loucks, R.G., Mescher, P.K., and McMechan, G.A., 2004, Three-dimensional architecture of a coalesced, collapsed-paleocave system in the Lower Ordovician Ellenburger Group, central Texas: American Association of Petroleum Geologists, Bulletin, v. 88, p. 545–564.

Matheron, G., Beucher, H., de Fouquet, C., Galli, A., Guerillot, D., and Ravenne, C., 1987, Conditional simulation of the geometry of fluvio-deltaic reservoirs: Society of Petroleum Engineers, Annual Technical Conference and Exhibition, SPE no. 16753.

McMechan, G.A., Loucks, R.G., Zeng, X., and Mescher, P., 1998, Ground penetrating radar imaging of a collapsed paleocave system in the Ellenburger dolomite, central Texas: Journal of Applied Geophysics, v. 39, p. 1–10.

McNeill, D.F., 2005, Accumulation rates from well-dated late Neogene carbonate platforms and margins: Sedimentary Geology, v. 175, p. 73–87.

Mescher, P., 1996, Architecture of collapsed-paleocave reservoirs (abstract): American Association of Petroleum Geologists Annual Meeting, A86 p.

Meyerhoff, A.A., and Hatten, C.W., 1974, Bahamian salient of North America: tectonic framework, stratigraphy and petroleum potential: American Association of Petroleum Geologists, Bulletin, v. 58, p. 1201–1239.

Muhs, D.R., 2002, Evidence for the timing and duration of the last interglacial period from high-precision uranium-series ages of corals on tectonically stable coastlines: Quaternary Research, v. 58, p. 36–40.

Mylroie, J.E., 1983, Cave and karst of San Salvador, *in* Gerace, D.T., ed., Field Guide to the Geology of San Salvador, Third Edition: College Center of the Finger Lakes, Bahamian Field Station: San Salvador, Bahamas, p. 67–91.

Mylroie, J.E., 1993, Carbonate deposition/dissolution cycles and carbon dioxide flux in the Pleistocene, *in* White, B., ed., Proceedings of the Sixth Symposium on the Geology of the Bahamas: Port Charlotte, Florida, Bahamian Field Station, p. 103–107.

Mylroie, J.E., and Carew, J.L., 1988, Solution conduits as indicators of late Quaternary sea level position: Quaternary Science Reviews, v. 7, p. 55–64.

Mylroie, J.E., and Carew, J.L., 1990, Flank margin model for dissolution cave development in carbonate platforms: Earth Surface Processes and Landforms, v. 15, p. 413–424.

Mylroie, J.E., and Carew, J.L., 1991, Erosional notches in Bahamian Carbonates: bioerosion or groundwater dissolution?, *in* Bain, R.J., ed., Proceedings of the Fifth Symposium on the Geology of the Bahamas: Port Charlotte, Florida, Bahamian Field Station, p. 85–90.

Mylroie, J.E., and Carew, J.L., 1995a, Geology and karst geomorphology on San Salvador Island, Bahamas: Carbonates and Evaporites, v. 10, p. 193–206.

Mylroie, J.E., and Carew, J.L., 1995b, Karst development on carbonate islands, *in* Budd, D.A., Saller, A.H., and Harris, P.M.M., eds., Unconformities and Porosity in Carbonate Strata: American Association of Petroleum Geologists, Memoir 63, p. 55–76.

Mylroie, J.E., Carew, J.L., Sealey, N.E., and Mylroie, J.R., 1991, Cave development on New Providence Island and Long Island, Bahamas: Cave Science, v. 18, p. 139–151.

Mylroie, J.E., Carew, J.L., and Vacher, H.L., 1995, Karst development in the Bahamas and Bermuda, *in* Curran, H.A., and White, B., eds., Terrestrial and Shallow Marine Geology of the Bahamas and Bermuda: Geological Society of America, Special Paper 300, p. 5–32.

Mylroie, J.E., Jenson, J.W., Taborosi, D., Jocson, J.M.U., Vann, D.T., and Wexel, C., 2001, Karst features of Guam in terms of a general model of carbonate island karst: Journal of Cave and Karst Studies, v. 63, p. 9–22.

Mylroie, J.E., Mylroie, J.R., and Jenson, J.W., 2004, Modeling carbonate island karst, *in* Martin, R., and Panuska, B., eds., Proceedings of the Eleventh Symposium on the Geology of the Bahamas and Other Carbonate Regions: San Salvador Island, Bahamas, Gerace Research Center, p. 135–144.

Operational Navigations Chart, 1974, Bahamas, Cayman Islands, Cuba, Haiti, Jamaica, Nassau Island, Sheet J26.

Palmer, A.N., 1991, Origin and morphology of limestone caves: Geological Society of America, Bulletin, v. 103, p. 1–21.

Palmer, R.J., McHale, M., and Hartlesbury, R., 1986, The caves and blue holes of Cat Island, Bahamas: Cave Science, v. 13, p. 71–86.
Plummer, L.N., 1975, Mixing of sea water with calcium carbonate ground water, *in* Whitten, E.H.T., ed., Quantitative Studies in Geological Sciences: Geological Society of America, Memoir 142, p. 219–236.
Roth, M.J., 2004, Inventory and geometric analysis of flank margin caves of the Bahamas [unpublished M. Sc. thesis]: Mississippi State University, 117 p.
Stoudt, E.L., 1996, Precambrian–Devonian geology of the Franklin Mountains, West Texas—analogs for exploration and production in Ordovician and Silurian Reservoirs in the Permian Basin: West Texas Geological Society, 1996 Annual Field Trip Guidebook, Publication 96-100, 220 p.
Vacher, H.L., 1988, Dupuit-Ghyben-Herzberg analysis of strip-island lenses: Geological Society of America, Bulletin, v. 100, p. 580–591.
White, W.B., 1988. Geomorphology and Hydrology of Karst Terrains: New York University Press, 464 p.
Wilson, W.L., 1994, Morphology and hydrology of the deepest known cave in the Bahamas: Dean's Blue Hole, Long Island: Abstracts and Program of the 7th Symposium on the Geology of the Bahamas, 21 p.

Received 6 January 2006; accepted 8 June 2007.